Fundamental Study of Optical Probe Current Sensor using Kerr Effect of Single Magnetic Domain Film

Makoto Sonehara, Naoki Otani, Takanori Goto,
Yusuke Kikuchi, Toshiro Sato, Kiyohito Yamasawa,
Yoshimasa Miura
Spin Device Technology Center
Shinshu University
Nagano, Nagano, Japan 380-8553
makoto@shinshu-u.ac.jp

Kazushi Asanuma
Department of Production Engineering
Nagano Prefectural Institute of Technology
Ueda, Nagano, Japan 386-1211
asanuma@pit-nagano.ac.jp

Abstract—An optical probe current sensor using a Kerr effect of an Fe-Si/Mn-Ir exchange-coupled film has been investigated. The optical sensing technique has the advantage of no induced noise from the external electromagnetic interference. In addition, since the proposed method using the Kerr effect of single domain exchange-coupled magnetic thin film utilizes only magnetization rotation, the Barkhausen noise due to a domain wall pinning can be excluded. A fabricated optical probe current sensor consisting of He-Ne laser, Fe-Si/Mn-Ir exchange-coupled film, beam splitter, pin-PD and differential amplifier, exhibited a current sensing bandwidth of 10 kHz and a sensitivity of 2.26 V/A. By using the fabricated optical probe current sensor, the current sensing for PWM inverter motor has been demonstrated.

I. INTRODUCTION

The electric vehicles and the hybrid vehicles have been developed for the environmental protection. A motor with an inverter is used in the vehicles, it is necessary to a detection of the motor current correctly for the control of the torque and the rotational frequency. Currently, a current sensor with the Hall element for the detection of the motor current has been used. However, the correct current sensing was difficult because the induced noise from an ignition and the inverter in the vehicles was transmitted to the sensor circuit. So the authors considered the optical probe current sensor using the Kerr effect of single magnetic domain film [1] without the electrical wire and the current sensor system in the vehicles as Fig. 1.
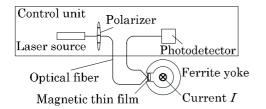
Figure 1. Configuration of the optical probe current sensor for the electric vehicles and the hybrid vehicles.

II. CONFIGURATION OF OPTICAL PROBE CURRENT SENSOR

Figure 2 shows a configuration of the optical probe current sensor and a circuit diagram for measuring a phase current I in a PWM inverter driven three-phase induction motor as described below. The current wire to measure the phase current I of the PWM inverter motor was coiled with 21 turns around the Mn-Zn ferrite core with a gap. And the Fe-Si/Mn-Ir exchange-coupled single domain film was placed in the gap. A direction of a magnetic field by I was corresponding to that of hard axis in the film. The Glan-Thompson polarizer was placed between the linearly polarized He-Ne Laser with $\lambda = 633$ nm and the film in order to improve the linearly polarization as Fig. 2. The incident plane of laser light was corresponding to the perpendicular plane of the direction of
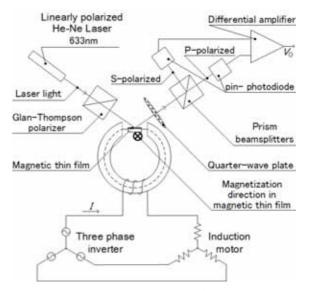
Figure 2. Configuration of the optical probe current sensor.

hard axis in the film. The reflected light from the film was split in P-polarized and S-polarized via the quarter-wave plate and the prism beamsplitters and it was incident on the pin-photodiodes. A principal axis of the quarter-wave plate was adjusted in order to equal the intensity of P-polarized and that of S-polarized when $I = 0$ (i.e. applied field $H = 0$). Then outputs from two pin-photodiodes were equal, so the output of the differential amplifier was 0. On the other hand, the intensity of P-polarized was not consistent with that of S-polarized in order to rotate the magnetic moment in the film when $I \neq 0$ (i.e. $H \neq 0$). Then outputs from two pin-photodiodes were not equal, so the differential amplifier had an output.

III. CHARACTERISTIC OF FE-SI/MN-IR EXCHANGE-COUPLED FILM

A. Ferro/Antiferromagneitc exchage coupling

An ferro/antiferromagnetic exchange-coupled film has two merits for the optical probe current sensor. First, the Barkhausen noise due to the domain wall pinning can be excluded in the exchange-coupled film. Because the film has a single magnetic domain because an exchange bias field is occurred in the ferromagnetic layer by an exchange-coupled energy in the interface of the ferromagnetic layer and the antiferromagnetic layer. So then mainly the magnetic property by a rotation of the magnetic moment is appeared, when the eternal field is applied an orthogonal direction of an exchange bias field H_{ex}. Second, the film has fast sensing because the limiting frequency of the magnetization rotation is extended to the ferromagnetic resonance frequency.

The exchange bias field H_{ex} and the static magnetic susceptibility χ in the hard axis of the exchange-coupled film are written as follows,

$$H_{ex} = \frac{J_{ex}}{t_F M_s}. \tag{1}$$

$$\chi = \frac{M_s}{H_k + H_{ex}}. \tag{2}$$

where J_{ex} is the exchange energy, t_F is the ferromagnetic layer thickness, M_s is the saturation magnetization and H_k is the uniaxial anisotropy magnetic field in the ferromagnetic layar. Since the static magnetic susceptibility χ can be changed easily by the ferromagnetic layer thickness t_F, so the sensitivity of the optical probe current sensor can be controlled by changing t_F.
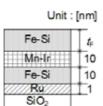

Figure 3. Cross-sectional structure of the Fe-Si/Mn-Ir exchange-coupled magnetic thin film.

In this study, Fe-Si/Mn-Ir exchange-coupled film was selected for the magnetic film using the Kerr effect, as shown in Fig.3. The details of the fabrication in the film had been reported in reference 2.

B. Reflection in Fe-Si/Mn-Ir exchange-coupled film

The reflection in the upper Fe-Si layer of the Fe-Si/Mn-Ir exchange-coupled film was investigated as shown in Fig. 4. The linearly polarized He-Ne Laser with $\lambda = 633$ nm was irradiated on the exchange-coupled film, then the light intensity of the reflection was measured by the laser power meter. And then it and the incident light intensity to the exchange-coupled film were compared. Figure 5 shows the Relationship between the reflection, the permeability μ and the upper Fe-Si thickness t_F in the Fe-Si/Mn-Ir/Fe-Si/Ru exchange-coupled film. In Fig. 5, the reflection has about 70 % which is not depended on the upper Fe-Si thickness t_F. On the other hand, when increasing the Fe-Si thickness t_F, the permeability μ increased, this reason is described in the previous section. When the exchange-coupled film has high permeability, large magnetization rotation was obtained by changing small magnetic filed (i.e. current), therefore high sensitivity of the optical probe current sensor can be obtained. Since in this paper, Fe-Si (100 nm)/Mn-Ir (10 nm)/Fe-Si (10 nm)/Ru (1 nm) film was selected.
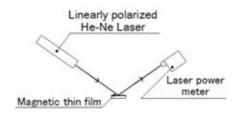

Figure 4. Schematic view of the reflection measurement for Fe-Si/Mn-Ir exchange-coupled film.
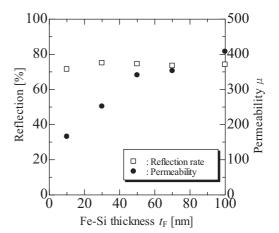

Figure 5. Relationship between reflection, permeability and upper Fe-Si thickness t_F in Fe-Si/Mn-Ir/Fe-Si/Ru exchange-coupled film.

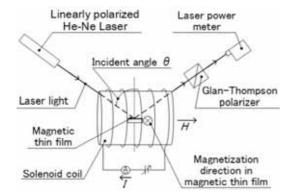## C. Mesurement of Kerr effect in Fe-Si/Mn-Ir exchange-coupled film

Figure 6 shows the schematic view of the Kerr effect measurement. The linearly polarized He-Ne Laser with $\lambda =$ 633 nm was utilized for the light source. The solenoidal coil was used for an excitation of dc magnetic field. And Fe-Si (100 nm)/Mn-Ir (10 nm)/Fe-Si (10 nm)/Ru (1 nm) exchange-coupled film was placed inside the solenoidal coil. The linearly polarized He-Ne Laser with $\lambda =$ 633 nm was irradiated on the exchange-coupled film with the incident angle θ, and then the reflected light from the film was passed into the Glan-Thompson polarizer, the light intensity was measured by the laser power meter as shown in Fig.6. The angle of the Glan-Thompson polarizer was adjusted to minimize the light intensity when $I = 0$ (i.e. $H = 0$). Then the magnetization was rotated when $I \neq 0$ (i.e. $H \neq 0$). Since the plane of polarization was rotated due to the Kerr effect, then the light intensity was changed. A difference between the light intensity in $I = 0$ and that in $I \neq 0$ was evaluated as ΔP.
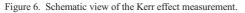
D. Relationship between incident angle and Kerr effect of Fe-Si/Mn-Ir exchange-coupled film

Figure 7 shows the relationship between the incident angle θ and the Kerr effect of the Fe-Si/Mn-Ir exchange-coupled film i.e. ΔP. In Fig. 7, ΔP peaks near $\theta = 55$ deg. As is well known [3], the Kerr rotation angle θ_k in the ferromagnetic material has peak in θ for $50 \leqq \theta \leqq 60$ [deg], so similar characteristic has been observed for Fe-Si/Mn-Ir exchange-coupled film.

E. Relationship between applied magnetic field and Kerr effect of Fe-Si/Mn-Ir exchange-coupled film

Figure 8 shows the relationship between the applied magnetic field H and ΔP in the the Fe-Si/Mn-Ir exchange-coupled film. The broken line makes the static magnetization curve in the hard axis measured for the Fe-Si/Mn-Ir exchange-coupled film in Fig. 8. In Fig. 8, the relationship between H and ΔP is approximately consistent with the static magnetization curve. And the laser intensity ΔP is approximately proportional to the applied field H for $-30 \leqq H \leqq 30$ [Oe]. Therefore, the current sensor with the linear response can be developing.
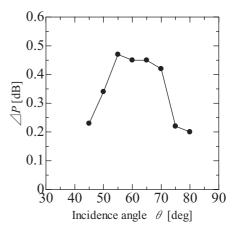
Figure 7. Relationship between incident angle θ and Kerr effect of the Fe-Si/Mn-Ir exchange-coupled magnetic film.
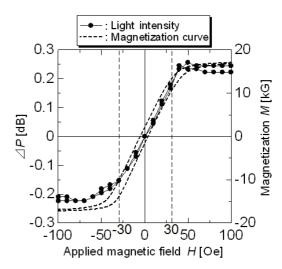
Figure 8. Relationship between Kerr effect and applied magnetic field H in the Fe-Si/Mn-Ir exchange-coupled magnetic film.

IV. PREPARATION AND CHARACTERIZATION OF OPTICAL PROBE CURRENT SENSOR

A. Photo detecting circuit of the optical probe current sensor

A differential method was adopted instead of the extinction method as described previous section in the configuration of the optical probe current sensor as shown in section 2 and Fig. 2.

Figure 9 shows the photo detecting circuit of the optical probe current sensor. The pin-photodiode with upper limit 20 MHz (Hamamatsu Photonics; S1223-01) was used. The backward bias current which is proportional to the light intensity was converted into the terminal voltage V_p by resistance R_p [4], and then it was inputted to the differential amplifier circuit.

Figure 10 shows the relationship between the terminal voltage V_P across the resistance R_P and the incident light

Figure 6. Schematic view of the Kerr effect measurement.

intensity of the pin-photodiode. In Fig. 10, the light intensity varies linearly with the terminal voltage V_p. In this study, the laser intensity was measured with 180 μW in the pin-photodiode, so then R_p^- and R_p^+ were adjusted to 10 kΩ, and the potentiometers R_{pp}^- and R_{pp}^+ were connected with R_p^- and R_p^+ in series respectively for fine control.

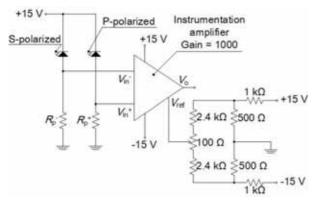
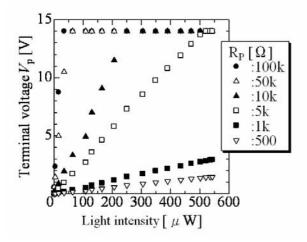Figure 9. Photo detecting circuit of the optical probe current sensor.

Figure 10. Relationship between voltage V_P across the resistance R_P and incident light intensity of the pin photodiode.

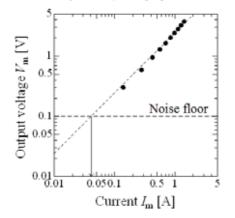Figure 11. Relationship between sensor output voltage V_m and current I_m at f = 1 kHz.

The signal of voltage from the pin-photodiode was inputted to the instrumentation amplifier with 1000 of an amplification factor (BURR-BROWN; INA118). The offset adjustment circuit was connected with V_{ref} in order to adjust an offset in the instrumentation amplifier as shown in Fig. 9. A cut-off frequency with 3 dB of the differential amplifier circuit was about 10 kHz.

B. Fundamental characteristics of the optical probe current sensor

The fundamental characteristics of the optical probe current sensor were measured when a current for dc to 100 kHz was flowed to the coil in the sensor as shown in Fig. 2. I was flowed by the function generator (NF; WAVE FACTORY 1952) was connected with the power amplifier (NF; 4055).

Figure 11 shows relationship between the amplitude of the sensor output voltage V_m and the amplitude of the current I_m at f = 1 kHz. The sensor output voltage V_m was a linear function of the current I_m. The noise floor in Fig. 11 corresponds to the sensor output noise in Fig. 12 when I = 0. It was considered that this reason for a dark current noise of the pin-photodiode and a noise in the circuit such as the differential amplifier. A detected limit current which was converted from the noise floor was estimated about 40 mA. Incidentally, the current I_m was limited 1.41 A in Fig. 11 because the limited current corresponds to a limited field for linear operation of the Kerr effect as shown in Fig. 8. A maximum current was depended on the gap length of the ferrite yoke and an inclination of the magnetization curve in the exchange-coupled film, so then it easily was controlled by these.
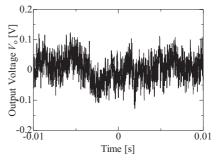

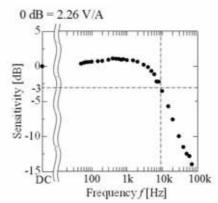Figure 12. Sensor output noise when current measured is zero.

Figure 13. Frequency characteristic of sensor sensitivity.
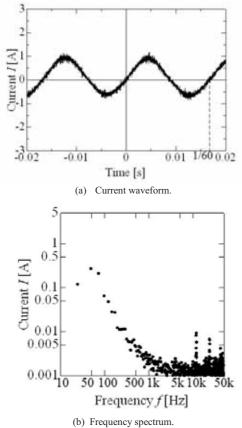
(a) Current waveform.

(b) Frequency spectrum.

Figure 14. Current waveform and its frequency spectrum of the PWM inverter driven three-phase induction motor, by using an optical probe current sensor.

(a) Current waveform.

(b) Frequency spectrum.

Figure 15. Current waveform and its frequency spectrum of the PWM inverter driven three-phase induction motor, by using a Hall element current probe.

Figure 13 shows the frequency characteristic of the sensor sensitivity. 3 dB cutoff frequency of sensor sensitivity was about 10 kHz. The sensing bandwidth was limited by the cutoff frequency of the differential amplifier, because the ferromagnetic resonance frequency in the Fe-Si/Mn-Ir exchange-coupled film has highly 1 GHz and the limit frequency of the pin-photodiode has 20 MHz. In order to obtain high cutoff frequency, it must establish lower amplitude gain or use wide band amplitude.
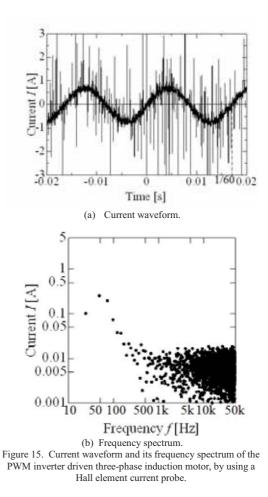
V. CURRENT MEASUREMENT OF PWM INVERTER DRIVEN THREE-PHASE INDUCTION MOTOR

A. Experimental method

The 200 W three-phase induction motor (HITACHI; CA19-020-10) was driven by the 12 kHz-PWM inverter (HITACHI; SJ100-002LFR) with 60 Hz. A phase current I of the PWM inverter driven induction motor was measured by the optical probe current sensor and a Hall element current probe (HIOKI; CT9277).

B. Experimental results

Figure 14 and 15 shows a current waveform and its frequency spectrum of the PWM inverter driven three-phase induction motor with 60 Hz of the driving frequency, by using the optical probe current sensor and the Hall element current probe. In Fig. 14, the square waveform with 60 Hz was obtained by using the optical probe current sensor. In Fig. 15 (a), a few spectrums of the carrier wave in the inverter with 12 kHz and its harmonic frequency were observed only. On the other hand, in Fig. 15 (b), high frequency spectrums were observed. Because the measurement band in the optical probe current sensor was limited to 10 kHz.

The fabricated optical probe current sensor in this research was limited the current measurement frequency for dc to 10 kHz because of the limited bandwidth in the differential amplifier. However, the current sensing in the inverter driven induction motor can be measuring to restrain an effects of carrier wave noise, because of a power supply frequency in the motor with a few kHz.

VI. CONCLUSION

The optical characteristics and the magnetic Kerr effect in the Fe-Si/Mn-Ir exchange-coupled film, the fundamental characteristics of the optical probe current sensor, and the current measurement of the PWM inverter driven three-phase induction motor were described for the fundamental investigation in the optical probe current sensor using Kerr

effect of the Fe-Si/Mn-Ir exchange-coupled film. The results obtained are as follows:

1) The linear response range with -30 $\leq H \leq$ 30 [Oe] was exhibied in Fe-Si (100 nm)/Mn-Ir (10 nm)/Fe-Si (10 nm)/Ru (1 nm) exchange-coupled single domain film.

2) The upper limit frequency for the current sensing was 10 kHz in the optical probe current sensor system because of the limited bandwidth in the differential amplifier. And the range of the current was measured 0.03 $\leq I \leq$ 1 [A].

3) The phase current of 12 kHz-PWM inverter driven three-phase induction motor was measured, and the frequency spectrum with low carrier wave noise in the phase current was observed because of the limited bandwidth in the differential amplifier.

In order to use this optical probe current sensor in general-purpose measurement, a wide sensing bandwidth in the circuit and an introduction of a semiconductor laser and an optical fiber for low cost are necessary.

REFERENCES

[1] M. Jimbo, "Present Status of Antiferromagnetic Materials in Spin Valves", Journal of Magnetics Society of Japan, vol.22, nr.1, pp.12-18, 1998.

[2] M. Sonehara, T. Sato, K. Yamasawa, Y. Miura, S. Ikeda, M. Yamaguchi, "Preparation and Characterization of Mn-Ir/Fe-Si Exchange-Coupled Film for High-frequency Micromagnetic Devices" Journal of Magnetics Society of Japan, Vol.29, No.2, pp.132-137, 2005.

[3] K. Sato, "Optical and Magnetics", Asakura Publishing, p. 50, 1988.

[4] S. Furukawa, M. Matsumura, "Electric devices [II]", Shokodo, pp. 10-12, 1980.